Catechol Derivatives as Fluorescent Chemosensors for Wide-Range pH Detection

Emilia Evangelio,[a] Jordi Hernando,[b] Inhar Imaz,[c] Gisela G. Bardají,[b] Ramon Alibés,[b] Félix Busqué,*[b] and Daniel Ruiz-Molina*[d]

Abstract: The synthesis and characterization of a new family of catechol derivatives designed to behave as fluorescent chemosensors for wide-range pH detection has been described. These compounds were prepared by covalently coupling a catechol unit with other aromatic rings, thus obtaining π-delocalized systems with both pH-responsive groups and fluorescent behavior. In the case of a pyridine–catechol derivative, this leads to up to three different protonation states with distinct optical properties in organic media, as corroborated by density functional theory calculations. By applying dual-wavelength detection techniques, this compound shows complementary "off–on–off" and "on–off–on" emission profiles upon pH variation, a behavior that can be exploited to perform acidity detection over a broad pH range.

Keywords: catechols · chemosensors · fluorescent probes · pH detection · switches

Introduction

In the last few years, the design, characterization, and device implementation of chemosensors has emerged as an active area of research owing to their wide-ranging applications in various fields of science and industry.[1] Because of its high sensitivity and selectivity as well as its noninvasive character, fluorescence is very often selected as the transduction signal for chemical sensing events.[2] Thus, great effort has been devoted to developing new materials for the luminescent detection of chemically and biologically relevant ions[3] and molecules.[4] Among them, fluorescent chemosensors that report on acidity changes are becoming increasingly interesting owing to the need for monitoring pH values in many chemical and biological processes, clinical analysis, and environmental-protection analyses.[5] In addition, pH-responsive molecular systems displaying optical activity have been proposed as logical operators to perform molecular computing.[6]

In contrast to glass electrodes, fluorescent chemosensors are usually not suitable for measurements over wide pH ranges, but they allow acidity detection in narrow pH-value windows.[5e–g] In fact, the dynamic range of most common chemosensors, which present only a single pH-responsive group leading to one fluorescent and one non-fluorescent state upon pH variation (i.e. "on–off" or "off–on" probes), is limited to approximately two pH units.[5f] Several strategies can be followed to broaden the sensing range of fluorescent pH chemosensors. On the one hand, this can be achieved by mixing different systems that respond to distinct pH values.[5f,g] More interestingly, pH detection over large intervals can also be attained with specific chemosensors, provided that they possess multiple pH-responsive groups that give rise to several protonation states with distinct optical properties.[5e,7] Multistate molecular systems displaying pH-induced "off–on–off"[7e,8] or "on–off–on"[9] fluorescence profiles are particularly relevant examples of this latter case. For "off–on–off" fluorescent pH chemosensors, minimal emission is detected in strongly acid and basic media, whereas maximal fluorescence is emitted at intermediate pH values. On the contrary, "on–off–on" systems become increasingly fluorescent at extreme pH values.

[a] E. Evangelio
Institut de Ciència de Materials de Barcelona (CSIC)
Esfera UAB, 08193, Cerdanyola del Vallès (Spain)

[b] Dr. J. Hernando, G. G. Bardají, Dr. R. Alibés, Dr. F. Busqué
Departament de Química, Universitat Autònoma de Barcelona
08193 Cerdanyola del Vallès (Spain)
Fax: (+34) 93-581-1265
E-mail: felix.busque@uab.es

[c] Dr. I. Imaz
Institut Català de Nanotecnologia, Edifici CM7 08193
Cerdanyola del Vallès (Spain)

[d] Dr. D. Ruiz-Molina
Centro de Investigación on Nanociencia y Nanotecnología
Edifici CM7, Campus UAB 08193, Cerdanyola del Vallès (Spain)
Fax: (+34) 93-580-1853
E-mail: druiz@cin2.es

The vast majority of multistate fluorescent pH chemosensors so far reported are complex molecular systems composed of a fluorophore and electronically uncoupled pH-sensitive units capable of modulating its luminescent properties. The mechanisms for such modulation are various, including photoinduced electron transfer and electronic energy transfer, among others.[5e,7–9] Alternatively, another approach has been the development of intrinsic fluorescent probes[2d] for wide-range pH detection, that is, chemosensors in which multiple pH-responsive groups are part of the π system of the fluorophore, whose inherent emissive properties therefore vary with pH. This allows a relatively simple synthesis of the chemosensors as well as an easier manipulation of the resulting structures.

Inspired by the behavior of well-known pH-responsive fluorescent probes such as fluorescein,[6a,10] our approach has consisted of the synthesis of new fluorophores that contain several groups with acid–base activity. Specifically, we have focused our attention on catechol derivatives because of its intrinsic acid–base properties ($pK_a = 9.2$ and 13.0 for pure catechol in water)[11] and their other interesting features. For instance, catechol derivatives have been successfully used in the design of molecular switches[12] and have significant implications in relevant biological processes such as the activation of small molecules like O_2 and N_2.[13] Herein, we describe the synthesis and the experimental and theoretical investigation of the optical properties of the catechol-derived compounds **1** and **2**. Compounds **1** and **2** have been prepared by covalently coupling a catechol unit with phenyl and pyridine moieties, respectively (see Scheme 1). π-Electron delocalization along both constituent groups is expected to lead to fluorescence emission in the visible region of the spectrum with a significant pH sensitivity thanks to the hydroxy groups of the catechol unit. More importantly, the additional acid–base activity of pyridine ($pK_a = 5.2$ for the pyridinium ion in water[14]) should make compound **2** a suitable fluorescent probe for acidity detection over a broad pH interval, as recently assessed.[15]
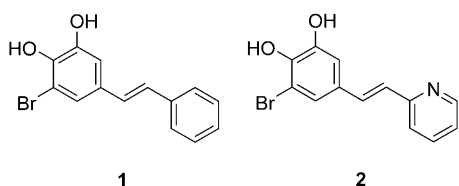

Scheme 1. Chemical structures of compounds **1** and **2**.

Results and Discussion

Synthesis: The sequence of reactions leading to target compounds began with commercially available 5-bromovanillin. Thus, cleavage of the methyl ether group of 5-bromovanillin by using anhydrous $AlCl_3$ in the presence of pyridine furnished catechol **3**[16] in 77% yield. Next, protection of the hydroxy groups of **3** as their *tert*-butyldiphenylsilyl (TBDPS)

derivatives was accomplished by using TBDPSCl and anhydrous 1,8-diazabicyclo[5.4.0]undec-7-ene (DBU) in a mixture of THF and N,N-dimethylformamide (DMF), affording compound **4** in 58% yield along with the monoprotected product **5** in 7% yield. This reaction failed when bases other than anhydrous DBU were used. A Wittig reaction of aldehyde **4** with benzyl-triphenylphosphonium chloride by using *t*BuOK as the base yielded an inseparable 1:2 mixture of the E and Z isomers of olefin **6** in 75% yield. This mixture was treated with triethylamine trihydrofluoride, affording a 1:2 mixture of the neutral form of the E and Z isomers of **1** in 78% yield (**n1**; Scheme 2). These isomers were separated by means of successive column chromatography. The isolated E isomer proved to be stable enough to be used for further experiments. On the contrary, the Z isomer isomerized back in a few days to the original (Z)- and (E)-**1** mixture even upon storage in the dark and at 4°C.
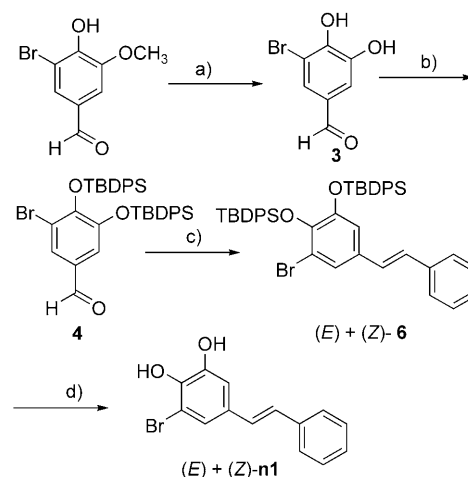
Scheme 2. Synthesis of compound **n1**: a) $AlCl_3$, pyridine, CH_2Cl_2, 24 h, reflux, 77%; b) TBDPSCl, DBU, THF/DMF, RT, 3 h, 58%; c) $(Ph)_3P^+$ CH_2-Ph Cl^-, *t*BuOK, THF, RT, 2 h, 75%; d) TEA/3HF, THF, RT, 2 h 78%.

Wittig reaction of intermediate **4** and triphenyl-(2-pyridyl-methyl)phosphonium chloride hydrochloride by using *t*BuOK as the base afforded (E)-olefin **7** in 83% yield. Final removal of the protecting silyl groups of **7** was achieved by using triethylamine trihydrofluoride, affording, after addition of 35% HCl, the hydrochloride salt of **2** in 65% yield (**c2**; Scheme 3). This yield decreased when tetrabutylammonium fluoride (TBAF) was used as a fluoride source for this reaction.

X-ray structure: All the attempts to obtain single crystals of **1** were unsuccessful in spite of the recurrent use of different crystallization techniques and solvents. More successful were the attempts to crystallize compound **2**. Yellow needles suitable for X-ray diffraction were obtained by slow evaporation of a solution of **2** in dichloromethane. Compound **2** crystallizes as the hydrochloride salt with one molecule in the asymmetric unit. Figure 1 shows the atom labeling and
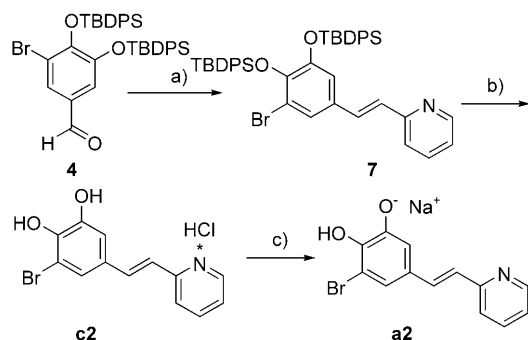
Scheme 3. Synthesis of compounds **c2** and **a2**: a) (Ph)₃P⁺CH₂-Py-HCl Cl⁻, *t*BuOK, THF, RT, 2 h, 83%; b) i) TEA-3HF, THF, RT, 2 h; ii) HCl 35%, 65%; c) 1 M NaOH, CH₂Cl₂, 94%.

Figure 2. Variation of the absorption spectrum of **1** upon pH increase in acetonitrile ($c_1 = 1 \times 10^{-5}$ M). The spectra shown were measured at pH values of 17.0, 17.7, 19.0, 20.5, 21.9, 22.4, 22.6, 23.1, 23.2, 23.5, and 24.0.

Table 1. Experimental and TD-DFT energies and intensities of the UV/Vis absorption bands of the different protonation states of **1** and **2**.

State	Solvent	Experimental[a]		TD-DFT[b,c]
		λ_{abs} [nm]	ε_{abs} [L mol⁻¹ cm⁻¹]	λ_{abs} [nm]
n1	THF	325	21259	
	acetonitrile	319	25098	346
	DMSO	329	20711	
a1	THF	398	24621	
	acetonitrile	388	30385	406
	DMSO	399	21274	
c2	THF	379	22248	
	acetonitrile	371	24558	408
	DMSO	382	22164	
n2	THF	334	25095	
	acetonitrile	327	26773	350
	DMSO	338	24178	
a2	THF	424	32169	
	acetonitrile	406	32362	422
	DMSO	421	28564	

[a] Measured at the absorption maxima. [b] B3LYP/6–311+G(d,p) level and accounting for acetonitrile solvent. [c] The ratios of the computed oscillator strengths (*f*) are: $f_{a1}/f_{n1} = 1.0$, $f_{c2}/f_{n2} = 0.8$, and $f_{a2}/f_{n2} = 1.0$.
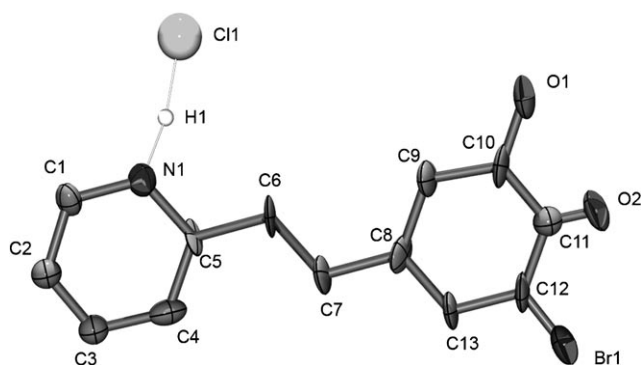

Figure 1. ORTEP view of the asymmetric unit of **2**. Hydrogen atoms, with the exception of the hydrogen atom that is implicated in the hydrogen bond with Cl1, are omitted for clarity.

the anisotropic displacement ellipsoids of **2**. The resolved structure is planar (C5-C6-C7-C8 dihedral angle 173°), and the intramolecular bond lengths and angles agree with those expected. Hydrochloric acid is connected to the molecule through a very strong hydrogen bond (N····Cl: 2.218 Å NHCl: 178.3 °). Although the molecular packing shows that the different molecules are organized in parallel rows, no π–π interactions are expected between them owing to the long intermolecular separation distance observed (5.583 Å). We ascribe this result to the presence of the voluminous halogenated atoms.

Acid–base equilibria: The acid–base activity of the catechol and phenyl/pyridine moieties in compounds **1** and **2** was investigated by UV/Vis absorption spectroscopy. Figure 2 displays the changes measured in the absorption spectrum of an acetonitrile solution of **n1** ($c_1 = 1 \times 10^{-5}$ M) upon base addition (tetrabutylammonium hydroxide; TBAH). Clearly, a new band at $\lambda_{abs} = 388$ nm appears with increasing pH, whereas the intensity of the initial peak at $\lambda_{abs} = 319$ nm decreases. Similar results are obtained in other solvents (Table 1). The absorption red-shift encountered upon base addition is consistent with the deprotonation of a hydroxy group in the neutral form **n1** to yield an anionic species
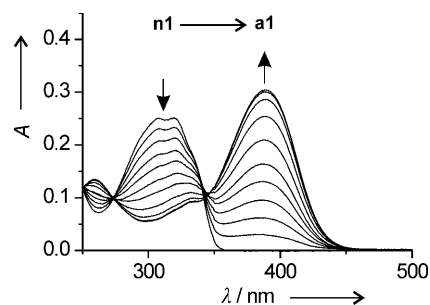
(**a1**), as previously reported for monohydroxystilbenes.[17,18] Importantly, this process can be fully reverted back upon acid addition (hydrochloric acid), thus recovering the absorption spectrum of **n1**.

The acid–base equilibrium between **n1** and **a1** is depicted in Scheme 4. Deprotonation to yield **a1** has been tentatively assigned to take place on the OH moiety at the *para* position of the catechol group according to inductive and conjugation considerations. This fact was confirmed by quantum-chemical calculations (see below). From the variations of the absorption spectra with pH,[19] an acidity constant value of pK_a = 22.6 has been determined for this process in acetonitrile, which is in good agreement with that reported for 2-bromophenol in the same solvent (pK_a = 23.9).[14] As the autoprotolysis constant of acetonitrile is p$K_{ACN} \geq 33$,[20] **n1** behaves as a weak acid in this solvent. Further basification of **a1** to yield the double phenolate form of **1** (pH > 25 in acetonitrile) was unsuccessful and resulted in irreversible degra-
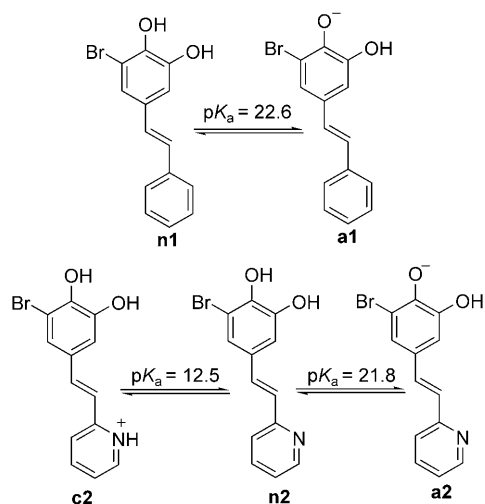
Scheme 4. Molecular structures of the neutral (**n1**) and anionic (**a1**) states of **1** as well as of the cationic (**c2**), neutral (**n2**), and anionic (**a2**) states of **2**. The acidity constants determined spectrophotometrically for the reversible acid–base equilibria between these states in acetonitrile are indicated.

dation of the compound, which we ascribe to either (photo-induced) addition of water to the ethylenic double bond[21] or a polymerization process.

A more complex acid–base activity was encountered for compound **2** (see Scheme 4). The absorption spectrum of a 1×10^{-5} M solution of **c2** in acetonitrile displays two different bands at $\lambda_{abs} = 327$ and 371 nm. The relative intensities of these bands varies with the addition of HCl and TBA with the peaks at 327 and 371 nm becoming predominant at pH 14.1 and 8.5, respectively (Figure 3). This indicates that even though complex **2** was originally in its cationic form, an equilibrium between the cationic form **c2** ($\lambda_{abs} = 371$) and its neutral state in which the pyridinium group is deprotonated (**n2**, $\lambda_{abs} = 327$) occurs in solution in acetonitrile. Interestingly, this process can be controlled and reversibly displaced forward or backwards by acid–base titration, as al-
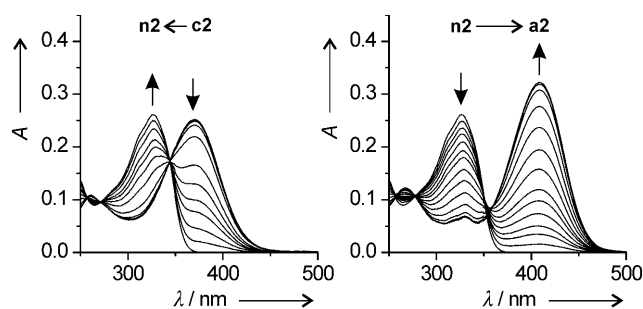

Figure 3. Variation of the absorption spectrum of **2** upon pH increase in acetonitrile ($c_2 = 1 \times 10^{-5}$ M). Left: The changes arising from the acid–base equilibrium between **c2** and **n2**, which were measured at pH values of 8.5, 9.9, 10.7, 11.4, 11.8, 12.4, 12.5, 12.6, 12.9, 13.0, 13.7, and 14.1. Right: The acid–base equilibrium between **n2** and **a2**, which were registered at pH values 14.1, 15.0, 16.9, 18.5, 19.8, 20.4, 20.9, 21.5, 22.2, 22.8, 23.1, 23.9, 24.2, and 24.8.

ready reported for related styrylpyridine compounds.[22–23] Moreover, from the variations of the absorption spectra with pH, an acidity constant value of $pK_a = 12.5$ has been determined for the deprotonation of the pyridinium group in acetonitrile. This result nearly matches the acidity constant reported for the pyridinium ion in acetonitrile ($pK_a = 12.3$–12.6) and it demonstrates the behavior of **c2** as a weak acid in this solvent.[14]

Subsequent deprotonation of **n2** to yield the anionic monophenolate state **a2** leads to additional variations in the absorption bands, as depicted in Figure 3. Such variations are indeed in agreement with those previously found for compound **1**, that is, red-shifted absorption upon base addition. This confirms deprotonation of the hydroxy group at the *para* position of the catechol moiety of **2** at larger pH values ($pK_a = 21.8$ in acetonitrile). Remarkably, this second acid–base equilibrium is also fully reversible, that is, the **a2** species can be reverted back to the **n2** species, making feasible the three-state device shown in Scheme 4. However, as already described for compound **1**, further basification to deprotonate the second -OH group of **2** leads to a degradation process (at pH > 25 in acetonitrile), thereby preventing reversible conversion of **a2** into the double anionic diphenolate form of this compound. Similar results are obtained in other solvents different from acetonitrile as summarized in Table 1 in which the experimental energies and intensities of the UV/Vis absorption bands of the different protonation states of **2** are shown.

Quantum-chemical calculations: Theoretical calculations were performed to further investigate the correspondence between the different absorption bands found in our spectrophotometric acid–base titration experiments and the distinct states of compounds **1** and **2**. Density functional theory (DFT) calculations employing the B3LYP hybrid functional and the 6–311+G(d,p) basis set and accounting for acetonitrile solvent were carried out to obtain the ground electronic state energies and optimal geometries of the different protonation states of **1** and **2**. Initially, computations of the monophenolate forms **a1** and **a2** in which the deprotonated hydroxy group was systematically modified to lay at either the *para* or *meta* position of the catechol moiety were performed. Noticeably, the ground electronic state energy of the former molecules (phenolate at the *para* position) was found to be approximately 10 kcal mol^{-1} lower in energy than that of the *meta* position. These results confirm the assignment of **a1** and **a2** to the structures shown in Scheme 4, thus demonstrating the larger acidity of the OH substituent at the *para* position of the catechol ring.

As is well-known for stilbene derivatives,[24] each one of the protonation states of **1** and **2** can present several different conformations associated with the rotation of the catechol and pyridine rings around the C1−C2 and C3−C4 bonds, respectively. This fact is illustrated in Scheme 5, in which the optimal geometries computed for the four possible rotamers of **c2** are shown (a, b, c, and d) as a representative example.
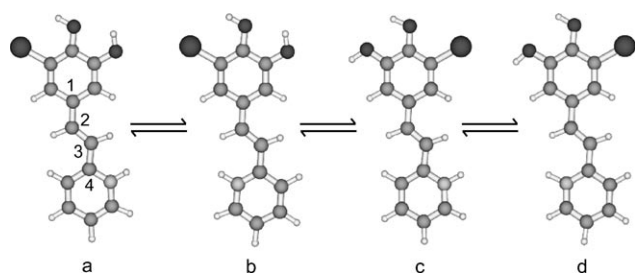
Scheme 5. Optimal geometries computed for the different rotamers of **c2** at the B3LYP/6–311+G(d,p) level and accounting for acetonitrile solvent. The ground-electronic-state energies of these conformers relative to that of *a* are 0 (a), 1.3 (b), −1.4 (c), and −0.1 kcal mol⁻¹ (d).

Similar planar structures were calculated for **n2** and **a2**. For **n1** and **a1**, only two different conformers are possible, which also present planar geometries. In all cases, our calculations yield very similar ground-electronic-state energies for all possible rotamers of a given protonation state of **1** and **2** (less than 2.5 kcal mol⁻¹ of difference). Thus, very small energy differences were computed for the four different rotamers of **c2** shown in Scheme 5, which fall below the accuracy of the calculation method employed. In spite of this, the occurrence of an equilibrium mixture of different rotamers in acetonitrile solution is anticipated, as previously observed for other stilbene derivatives.[24] This has been confirmed by means of NMR spectroscopy measurements. ROESY spectroscopy experiments of **c2** in deuterated dimethyl sulfoxide (DMSO) show a nuclear Overhauser effect (NOE) between both ethylenic protons and all the hydrogen atoms at the *ortho* positions of the pyridine and catechol rings. Together with the presence of only one series of proton signals in the ¹H NMR spectrum, this indicates the occurrence of a dynamic equilibrium between different rotational conformers in solution and at room temperature. An average behavior is therefore measured in our spectroscopic experiments.

Finally, time-dependent functional theory (TD-DFT) calculations at the B3LYP/6–311+G(d,p) level and accounting for acetonitrile solvent were carried out to compute the excitation energies and oscillator strengths of the absorption bands of the different protonation states of **1** and **2**. To account for conformational equilibria, TD-DFT calculations on the ground-electronic-state optimal geometries of all possible rotamers were performed. Although minor differences of their spectroscopic parameters were observed for a given protonation state, the final values of absorption energies and oscillator strengths were averaged over all possible rotamers by taking into account the Boltzmann distribution of conformer populations at room temperature. The resulting values are compared with the experimental ones in Table 1. As can be seen, a good agreement between quantum-chemical calculations and spectrophotometric measurements is observed. Thus, our computations reproduce, to a good extent, the spectral shifts obtained experimentally upon pH variation as the deviations between the calculated excitation energies and the experimental absorption maxima (in energy

units) fall below 10% in all cases. We partly ascribe these differences to the polarizable continuum model employed to account for acetonitrile solvent. Although this method allows accurate description of the electrostatic solvent effects, it does not consider the microscopic interactions between the solute and solvent molecules, such as hydrogen-bond formation.[25] Proper evaluation of all these solvent effects would require computationally demanding calculations in which both continuum and discrete solvation models were considered.[25]

On the other hand, TD-DFT calculations also reveal that the absorption transitions measured occur between the HOMO and LUMO states of all investigated molecules. These frontier orbitals are delocalized over both the catechol and phenyl/pyridine rings, thereby explaining why the absorption spectrum changes upon protonation/deprotonation of substituents located in any of the two constituent units of compounds **1** and **2**.

pH-modulated fluorescence: The emission properties of the different protonation states of compounds **1** and **2** have been evaluated. According to their stilbene character, the different protonation states derived from them exhibit fluorescence. The fluorescence spectral maxima (λ_f) and quantum yields (Φ_f) measured on different solvents are shown in Table 2, whereas the corresponding fluorescence spectra in acetonitrile are given in Figure 4. Clearly, **n1** and **a1** as well as **c2**, **n2**, and **a2** show distinct emissive behaviors, which confirm their potential use as fluorescent pH chemosensors.

Both the neutral forms of **1** and **2** display a large red-shift in fluorescence spectra upon deprotonation (≈ 100 nm), as previously observed for related monohydroxystilbenes[17,18] and in the absorption measurements. Similarly, protonation

Table 2. Fluorescence properties of the different protonation states of **1** and **2**.

State	Solvent[a]	λ_f [nm][b]	Φ_f
n1	THF	388	0.065
	acetonitrile	392	0.031
	DMSO	414	0.072
a1	THF	488	0.036
	acetonitrile	484	0.066
	DMSO	501	0.054
c2	THF	500	0.19
	acetonitrile	511	0.069
	DMSO	501	< 0.01
n2	THF	406	0.097
	acetonitrile	409	0.053
	DMSO	442	0.34
a2	THF	523	0.20
	acetonitrile	524	0.22
	DMSO	532	0.36

[a] Solvent dielectric constants are $\varepsilon_{THF}=7.5$, $\varepsilon_{ACN}=36.6$, and $\varepsilon_{DMSO}=47.2$, whereas the Kamlet–Taft β factors accounting for their hydrogen-bond acceptor capacity are $\beta_{THF}=0.55$, $\beta_{ACN}=0.31$, and $\beta_{DMSO}=0.76$.[26] [b] Measured at the emission maxima.
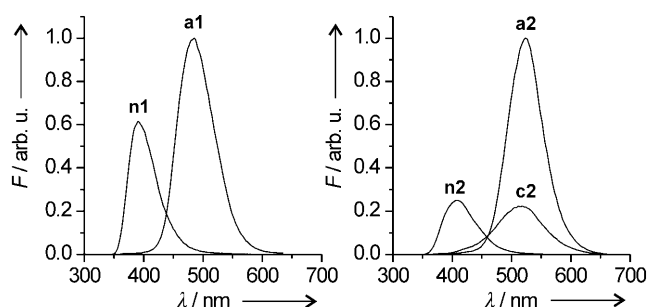
Figure 4. Fluorescence emission spectra of the different protonation states of compounds **1** ($\lambda_{exc} = 280$ nm, $c_1 = 1 \times 10^{-5}$ M) and **2** ($\lambda_{exc} = 310$ nm, $c_2 = 1 \times 10^{-5}$ M) in acetonitrile. Each spectrum is normalized with respect to the absorption at the excitation wavelength. Acid (HCl) or base (TBA) was added to adjust the pH of the solution to the values at which full conversion into the desired protonation state was achieved in each case: pH 17.0 (**n1**), 24.0 (**a1**), 8.5 (**c2**), 14.5 (**n2**), and 24.0 (**a2**).

of **n2** to yield **c2** not only leads to bathochromic absorption, but additionally results in red-shifted fluorescence, which is in agreement with previous reports on the luminescence of related styrylpyridine compounds.[22,23] Solvatochromic effects on the fluorescence spectra of compounds **1** and **2** are also observed, which we ascribe to both changes in solvent polarity as well as in solvent hydrogen-bond accepting capacity, as quantified by means of the Kamlet–Taft β factor.[26] Thus, similar fluorescence maxima are, in general, observed in THF and acetonitrile as the higher hydrogen-bond accepting capacity of the former ($\beta_{THF} = 0.55$, $\beta_{ACN} = 0.31$) is counterbalanced by the larger polarity of the latter ($\varepsilon_{THF} = 7.5$, $\varepsilon_{ACN} = 36.6$). In case of DMSO as the solvent, its higher ε ($\varepsilon_{DMSO} = 47.2$) and β ($\beta_{DMSO} = 0.76$) values lead to red-shifted emission for **n1**, **a1**, **n2**, and **a2**. Opposite behavior is found for **c2**, for which larger hydrogen-bond interaction between the pyridinium group and THF or DMSO molecules results in hypsochromic displacement of the emission spectrum. Our experimental data show that fluorescence quantum yields also vary for different solvents and protonation states of **1** and **2** (see Table 2).

In the case of compound **1**, both **n1** and **a1** states present relatively low Φ_f values within the 0.03–0.07 range. However, while larger fluorescence quantum yields are obtained for **n1** in solvents with high hydrogen-bond accepting capacity (THF and DMSO), an opposite trend is observed for **a1**. Most importantly, larger Φ_f values are determined for **2** under selected conditions, which is a relevant feature for potential fluorescent-sensing applications. This contrasts with previous studies on the effect of introducing a nitrogen atom in the styryl system, in which a decrease in fluorescence emission from stilbene to 2-styrylpyridine was observed.[27] Most probably, this difference arises from the effect of the hydroxyl group and bromo substituents of the catechol ring. Indeed, a tenfold increase in Φ_f has been reported for 3-hydroxystilbene with respect to stilbene in organic solvents,[17] thus demonstrating the critical effect of *meta* substitution with OH moieties on the photochemical properties of styryl systems. Consequently, the combined

effect of the nitrogen atom and the substitution of the hydroxyl group must account for the larger values of Φ_f that are typically obtained in this work for **2** with respect to **1** and stilbene ($\Phi_f = 0.04$ in hexane[27]).

All protonation states of compound **2** display significant solvent effects on their fluorescence quantum yields. In the case of **c2**, a Φ_f value as high as 0.19 is determined in THF. Nevertheless, increasing solvent polarity results in a dramatic decrease in fluorescence quantum yield, which leads to nearly complete suppression of emission for polar solvents such as DMSO (see Table 2), DMF, ethanol, and water (data not shown). A different behavior is encountered for the neutral state **n2**, whose fluorescence quantum yield rises with increasing hydrogen-bond accepting capacity of the solvent, as also observed for **n1**. Unfortunately, such large emission efficiencies of **n2** in organic media are lost in aqueous solutions, as has previously been reported for other hydroxystilbenes.[17] For the anionic form **a2**, solvent effects on the fluorescence quantum yield seem less important because large and similar Φ_f values are measured in THF, acetonitrile, and DMSO. In this case, however, major effects are encountered when **a2** is dissolved in solvents with hydrogen-bond donor capacity that can interact with the deprotonated hydroxy group of the phenolate. This results in very low Φ_f values (data not shown). Thus, for instance, aqueous solutions of **a2** in water are nearly not fluorescent, as also observed for **c2** and **n2**. In spite of this, the large emission efficiencies and different spectral properties observed for these species in several other solvents allows us to envisage compound **2** as a potential fluorescent pH chemosensor in organic media.

Fluorescence pH-sensing: If a wide-range pH sensor based on compound **2** is to be achieved, the capacity of this species to univocally respond to acidity changes over a large interval of pH values must be proved. Herein we discuss how the pH-sensitive fluorescence properties of **2** can be exploited to ensure the accomplishment of this condition.

In the previous section, we have shown that the fluorescence spectrum of the neutral form **n2** is approximately 100 nm blue-shifted with respect to **c2** and **a2**, whereas these two ionic species emit in the same spectral region but with different quantum yields (see Figure 4). As a consequence, if selective detection at the maximum of the emission spectrum of **n2** is performed (≈ 400 nm), the fluorescence signal measured will be maximal at intermediate pH values and it will decrease for increasingly acid or basic media. This means that compound **2** behaves as an "off–on–off" pH sensor under such detection conditions,[7e, 8] as is depicted in Figure 5 a. On the contrary, if the fluorescence detection window is centred on the maximum of emission of **c2** and **a2** (≈ 500 nm), the response of the system upon pH variation becomes of the "on–off–on" type.[9] Therefore, maximal fluorescence signal is detected at extreme values of pH in this case, as also illustrated in Figure 5 a. In Figure 5 a, the fluorescent "off–on–off" and "on–off–on" behaviors of **2** in acetonitrile at different detection conditions are compared
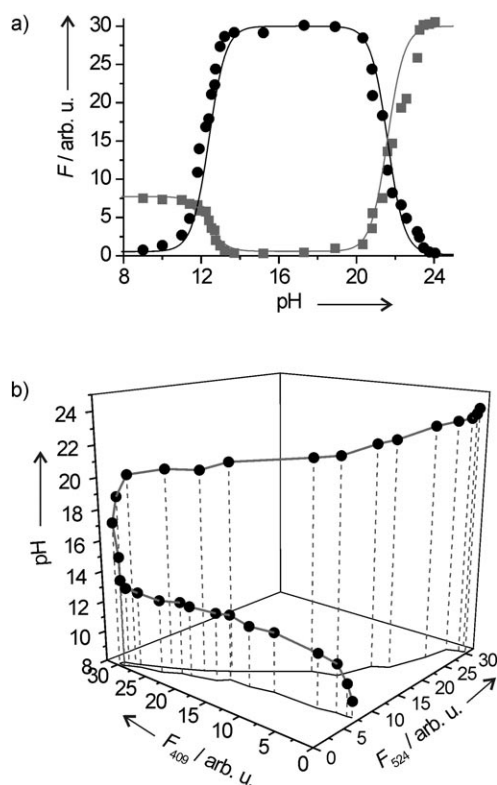
Figure 5. a) pH dependence of the fluorescence intensity (F) of **2** in acetonitrile ($\lambda_{exc} = 310$ nm, $c_2 = 1 \times 10^{-5}$ M) at $\lambda_{em} = 409$ nm (black) and $\lambda_{em} = 524$ nm (gray). Experimentally measured intensities are represented as points shown on the graphs. The solid lines plot the simulated emission intensities that were computed by using the pK_a constants, absorption extinction coefficients, and fluorescence quantum yields determined for **2** in acetonitrile. b) 3D plot showing the correspondence between pH and the fluorescence intensities measured for **2** in acetonitrile by means of dual-wavelength detection at $\lambda_{em} = 409$ and 524 nm (F_{409} and F_{524}).

with simulations performed by using the values of pK_a, absorption extinction coefficients, and fluorescence quantum yields that were previously determined for this species. Clearly, a good agreement exists between the simulated and experimental data. Thus, the dependence of fluorescence intensity at $\lambda_{em} = 409$ nm is rather symmetric around pH 17, as expected from the calculations. More importantly, an asymmetric curve describes the variation of the emission intensity with pH at $\lambda_{em} = 524$ nm, which arises from the different Φ_f values of **c2** and **a2**. This situation contrasts with the behavior observed for previously reported fluorescence "on–off–on" systems.[9]

The coexistence of the fluorescent "off–on–off" and "on–off–on" behaviors of **2** in acetonitrile at different detection conditions is an excellent scenario for the development of the sensing routine. Fluorescent molecular chemosensors exclusively displaying "off–on–off" or "on–off–on" profiles are mainly suited for the detection of pH windows. Unfortunately, they can hardly provide any information on the pH values at which point the system is "off", thus preventing the device from sensing over larger pH intervals. This drawback can be overcome by the use of **2** as the fluorescent pH probe as this compound shows both "off–on–off" and "on–off–on" responses upon pH variation when dual-wavelength detection is applied. However, this condition is not sufficient for univocal pH sensing. To be capable of discerning low from high pH values at which the fluorescence of the system simultaneously turns "off" (at $\lambda_{em} \approx 400$ nm) or "on" (at $\lambda_{em} \approx 500$ nm), the compound must display an asymmetric "on–off–on" profile, that is, it must show different luminescent properties at those two pH ranges. As mentioned above, this is accomplished by **2** in some organic media owing to the different fluorescence quantum yields of the **c2** and **a2** states. Consequently, each pH value will result in an univocal set of emission intensities at the two monitored wavelengths. This is demonstrated by the 3D plot in Figure 5 b, which shows the correspondence between pH values and the fluorescence intensities measured for **2** in acetonitrile at two different emission wavelengths, $\lambda_{em} = 409$ nm (F_{409}) and 524 nm (F_{524}). Remarkably, a single value of pH can be recovered from a given pair of F_{409} and F_{524} values measured by means of dual-wavelength detection. Therefore, we envisage compound **2** as a potential acidity chemosensor over large pH intervals in organic media. Furthermore, because of the fluorescent nature of all protonation states of this species, future application of compound **2** for pH detection could benefit from the use of ratiometric methods, thus preventing the need for prior calibration of the sensing system.[5d,f,7d]

Conclusion

Herein we describe the synthesis and characterization of a new chemosensor for a wide-range pH detection based on a fluorescent system decorated with several pH-responsive groups. With this aim, two catechol derivatives were prepared by covalently coupling a catechol unit to phenyl (**1**) and pyridine (**2**) rings. This led to π-delocalized systems that display pH-sensitive fluorescence emission in the visible region. Although **1** presents two stable protonation states with distinct optical properties, both experimental measurements and DFT calculations reveal that compound **2** shows up to three different luminescent protonation states in organic media owing to the combined acid–base activity of its constituent catechol and pyridine units. Importantly, the optical behavior of these states is such that compound **2** displays complementary "off–on–off" and "on–off–on" emission profiles upon pH variation by applying dual-wavelength detection techniques. This not only allows application of ratiometric methods, but, more importantly, it can be exploited to perform acidity detection over a broad pH range in organic solvents.

Experimental Section

General procedures: Commercially available reagents were used as received. The solvents were dried by distillation over the appropriate

drying agents. All reactions were performed avoiding moisture by standard procedures and under nitrogen atmosphere and monitored by analytical thin-layer chromatography (TLC) by using silica gel 60 F$_{254}$ precoated aluminum plates (0.25 mm thickness). Flash column chromatography was performed by using silica gel 60 Å, particle size 35–70 μm. NMR spectroscopy experiments were performed at the Servei de Ressonància Magnètica Nuclear of the Universitat Autònoma de Barcelona. ^{1}H NMR spectra were recorded on Bruker DPX250 (250 MHz) and Bruker DPX360 (360 MHz) spectrometers. Proton chemical shifts are reported in ppm (δ) (CDCl$_3$, δ = 7.26 ppm or [D$_6$]DMSO, δ = 2.50 ppm). ^{13}C NMR spectra were recorded on Bruker DPX250 (62.5 MHz) and Bruker DPX360 (90 MHz) spectrometers with complete proton decoupling. Carbon chemical shifts are reported in ppm (δ) (CDCl$_3$, δ = 77.2 ppm or [D$_6$]DMSO, δ = 39.5 ppm). NMR signals were assigned with the help of COSY, HSQC, HMBC, and NOESY experiments. Infrared spectra were recorded on a Sapphire-ATR spectrophotometer; peaks are reported in cm^{-1}. High-resolution mass spectra (HRMS) were recorded at Micromass-AutoSpec by using (ESI+ or ESI−).

3-Bromo-4,5-dihydroxybenzaldehyde (3):[16] Anhydrous aluminum chloride (3.2 g, 23.8 mmol) was suspended in a solution of 5-bromovanillin (5.0 g, 21.6 mmol) in CH$_2$Cl$_2$ (50 mL). While cooling to maintain the temperature at 30–35°C, pyridine (7.7 mL, 95.2 mmol) was added slowly. The resulting clear solution was heated to reflux for 24 h, allowed to warm to room temperature, quenched by the slow addition of 10% HCl solution (60 mL), and further diluted with CH$_2$Cl$_2$ (30 mL). The resulting suspension was filtered to afford catechol **3** as a white solid (3.60 g, 16.6 mmol; 77%). M.p. 225–227°C.

3-Bromo-4,5-bis(*tert*-butyldiphenylsilyloxy)benzaldehyde (4): DBU (6.5 mL, 43.8 mmol) was added dropwise over 20 min to a stirred solution of **3** (3.8 g, 17.5 mmol) and TBDPSCl (10.5 mL, 40.3 mmol) in a mixture of dry THF (100 mL) and anhydrous DMF (20 mL) at 0°C. After the mixture had been stirred at room temperature for 3 h, ethyl ether (100 mL) was added and the resulting suspension filtered. The filtrate was concentrated under vacuum and the resulting yellowish wax was purified by column chromatography on silica gel (gradient, hexanes/CH$_2$Cl$_2$ 4:1 to 1:1) to afford the following fractions: i) 3-bromo-4,5-bis(*tert*-butyldiphenylsilyloxy)benzaldehyde (**4**) as a solid (7.10 g, 10.2 mmol; 58%); and ii) 3-bromo −5-(*tert*-butyldiphenylsilyloxy)-4-hidroxybenzaldehyde (**5**) as a solid (0.56 g, 1.20 mmol; 7%). **4**: m.p. 151–153°C (ethyl ether); ^{1}H NMR (250 MHz, CDCl$_3$): δ = 9.29 (s, 1H), 7.83–7.72 (m, 4H), 7.61 (d, J = 1.9 Hz), 7.53–7.20 (m, 16H), 6.86 (d, J = 1.9 Hz), 1.13 (s, 9H), 0.76 ppm (s, 9H); ^{13}C NMR (62.5 MHz, CDCl$_3$): δ = 189.4, 149.3, 147.6, 135.5, 135.3, 133.0, 132.0, 130.1, 130.0, 129.9, 127.9, 127.8, 127.3, 122.2, 117.0, 27.1, 26.4, 20.7, 19.3 ppm; IR (ATR): $\tilde{\nu}$ = 3267, 2930, 2856, 1669, 1428, 1314, 1300, 1100, 885, 701 cm^{-1}; HRMS (ESI): m/z: [M+2+Na$^+$]$^+$ calcd for C$_{39}$H$_{41}$BrNaO$_3$Si$_2$ 717.1657; found: 717.1640. **5**: m.p. 126–127°C (ethyl ether); ^{1}H NMR (250 MHz, CDCl$_3$): δ = 9.42 (s, 1H), 7.75–7.64 (m, 4H), 7.60 (d, J = 1.7 Hz, 1H), 7.53–7.34 (m, 6H), 6.84 (d, J = 1.7 Hz, 1H), 6.57 (s, 1H), 1.15 ppm (s, 9H); ^{13}C NMR (62.5 MHz, CDCl$_3$): δ = 189.3, 150.3, 143.5, 135.5, 130.9, 129.8, 128.5, 128.4, 117.9, 109.2, 26.8, 19.7 ppm; IR (ATR): $\tilde{\nu}$ = 2960, 2856, 1696, 1424, 1310, 1107, 917, 870, 697 cm^{-1}; HRMS (ESI+): [M+2+Na$^+$] calcd for C$_{23}$H$_{23}$BrNaO$_3$Si 479.0475; found: 479.0464.

(*E*)-3-Bromo-5-(2-phenyl-1-ethenyl)-1,2-di(*tert*-butyldiphenylsilyloxy)-benzene (6): *t*BuOK (0.419 g, 3.75 mmol) was added portionwise at 0°C to a solution of benzyltriphenylphosphonium chloride (1.23 g, 3.17 mmol) in dry THF (25 mL). After the mixture had been stirred for 30 min at room temperature, a solution of **4** (2.0 g, 2.88 mmol) in dry THF (5 mL) was added. The mixture was stirred for 2 h at room temperature, quenched with brine (0.3 mL), diluted with ethyl ether (20 mL), and filtered. The filtrate was concentrated under vacuum and the resulting crude material was purified by column chromatography on silica gel (gradient, hexanes/CH$_2$Cl$_2$ 5:1 to 3:1) to afford a 1:2 mixture of *E* and *Z* isomers of 3-bromo-5-(2-phenyl-1-ethenyl)-1,2-di(*tert*-butyldiphenylsilyloxy)benzene (**6**) as a wax (1.65 g, 2.15 mmol; 75%). ^{1}H NMR (360 MHz, CDCl$_3$): δ = 7.88–7.70 (m, 4H), 7.50–6.90 (m) + 6.84 (d, J = 1.8 Hz, *Z*) (22H), 6.56 (d, J = 1.8 Hz, *E*) + 6.26 (d, J = 1.8 Hz, *Z*) (1H), 6.49 (d, J = 16.2 Hz, *E*) + 6.22 (d, J = 12.2 Hz, *Z*) (1H), 6.05 (d, J = 16.2 Hz, *E*) +

5.89 (d, J = 12.2 Hz, *Z*) (1H), 1.09 (s, *E*) + 1.07 (s, *Z*) (9H), 0.76 (s, *E*) + 0.73 ppm (s, *Z*) (9H); ^{13}C NMR (90 MHz, CDCl$_3$): δ = 147.2, 147.1, 143.4, 143.0, 137.3, 136.7, 135.6, 135.5, 135.4, 133.7, 133.01, 132.8, 130.9, 130.8, 130.0, 129.9, 129.8, 129.7, 129.7, 128.9, 128.7, 128.4, 128.2, 128.1, 127.9, 127.8, 127.7, 127.6, 127.2, 126.8, 126.4, 125.9, 124.8, 121.7, 118.3, 116.0, 115.7 ppm; HRMS (ESI+): m/z: [M+Na]$^+$ calcd for C$_{46}$H$_{47}$BrNaO$_2$Si$_2$ 791.2180; found: 791.2168.

(*E*)-3-Bromo-5-(2-phenyl-1-ethenyl)-1,2-benzenediol (n1): Triethylamine trihydrofluoride (0.63 mL, 3.92 mmol) was added dropwise at 0°C to a solution of **6** (1.50 g, 1.96 mmol) in dry THF (20 mL). The mixture was stirred for 2 h at room temperature, quenched with brine (0.3 mL), diluted with ethyl ether (20 mL), and filtered. The filtrate was concentrated under vacuum and the resulting crude material was purified by chromatography on silica gel (gradient, hexanes/CH$_2$Cl$_2$ 5:1 to 3:1) to afford a 1:2 mixture of *E* and *Z* isomers of 3-bromo-5-(2-phenyl-1-ethenyl)-1,2-benzenediol (**7**) as a solid (0.443 g, 1.52 mmol; 78%). Repeated column chromatography allowed isolation of the pure *E* isomer and a *Z*-enriched mixture (4:1) of isomers. (*E*)-**8**: m.p. 95–96°C (ethyl ether); ^{1}H NMR (250 MHz, CDCl$_3$): δ = 7.50–7–39 (m, 2H), 7.39–7.28 (m, 2H), 7.28–7.18 (m, 1H), 7.14 (d, J = 2.7 Hz, 1H), 7.03 (d, J = 2.7 Hz, 1H), 6.93 (d, J = 16.3 Hz, 1H), 6.86 (d, J = 16.3 Hz, 1H), 5.52 ppm (br s, 2H); ^{13}C NMR (62.5 MHz, CDCl$_3$): δ = 144.7, 139.9, 137.2, 132.2, 128.9, 128.6, 127.9, 127.0, 126.6, 121.9, 112.8, 109.9 ppm; IR (ATR): $\tilde{\nu}$ = 3422, 3356, 1590, 1521, 1427, 1291, 959, 858, 830, 750, 692 cm^{-1}; HRMS (ESI): m/z: [M−H$^+$]$^-$ calcd for C$_{14}$H$_{10}$BrO$_2$ 288.9859; found: 288.9861. Mixture (4:1) of (*Z*)- and (*E*)-**7** isomers: ^{1}H NMR (360 MHz, CDCl$_3$): δ = 7.50–7.43 (m, *E*) + 7.39–7.31 (m, *E*), 7.30–7.15 (m) (5H), 7.17 (d, J = 1.8 Hz, *E*) + 7.06 (d, J = 1.8 Hz, *E*) + 6.75 (d, J = 1.6 Hz, *Z*) + 6.92 (d, J = 1.6 Hz, *E*) (2H), 6.96 (d, J = 16.2 Hz, *E*) + 6.90 (d, J = 16.2 Hz, *E*) + 6.55 (d, J = 12.0 Hz, *Z*) + 6.40 (d, J = 12.0 Hz, *Z*) (2H), 5.52 (br s, *E*) + 5.48 (br s, *Z*) + 5.39 (br s, *Z*) + 5.29 ppm (br s, *E*) (2H); ^{13}C NMR (90 MHz, CDCl$_3$): δ = 144.7, 144.1, 139.9, 139.5, 137.2, 137.0, 132.2, 131.6, 130.6, 129.0, 128.9, 128.6, 128.5, 128.5, 127.9, 127.5, 127.0, 126.6, 124.1, 121.9, 115.5, 112.8, 109.9, 109.3 ppm.

(*E*)-2-[3-Bromo-4,5-di(*tert*-butyldiphenylsilyloxy)phenyl]-1-ethenyl]pyridine (7): *t*BuOK (1.11 g, 9.94 mmol) was added portionwise at 0°C to a solution of triphenyl-(2-pyridylmethyl)phosphonium chloride hydrochloride (1.84 g, 4.32 mmol) in dry THF (40 mL). After the mixture had been stirred for 30 min at room temperature, a solution of **4** (3.0 g, 4.32 mmol) in dry THF (10 mL) was added. The mixture was stirred for 2 h at room temperature, quenched with brine (0.5 mL), diluted with ethyl ether (30 mL), and filtered. The filtrate was concentrated under vacuum and the resulting crude material was purified by flash chromatography on silica gel (gradient, hexanes/EtOAc 6:1 to 4:1) to afford (*E*)-2-[3-bromo-4,5-di(*tert*-butyldiphenylsilyloxy)phenyl]-1-ethenyl]pyridine (**7**) as a solid (2.76 g, 3.58 mmol; 83%). M.p. 182–185°C (ethyl ether); ^{1}H NMR (360 MHz, CDCl$_3$): δ = 8.52–8.47 (m, 1H), 7.81–7.75 (m, 4H), 7.56 (dt, J = 7.9 Hz, J = 1.8 Hz, 1H), 7.45–7.20 (m, 16H), 7.22 (d, J = 2.2 Hz, 1H), 7.07 (d, J = 15.8 Hz, 1H), 7.09–7.02 (m, 1H), 7.02 (d, J = 7.9 Hz, 1H), 6.60 (d, J = 2.2 Hz, 1h), 6.21 (d, J = 15.8 Hz, 1H), 1.10 (s, 9H), 0.75 ppm (s, 9H); ^{13}C NMR (90 MHz, CDCl$_3$): δ = 155.4, 149.7, 147.2, 144.0, 136.6, 135.5, 135.4, 133.6, 132.8, 130.9, 130.3, 129.9, 129.7, 127.9, 127.7, 127.1, 125.1, 122.6, 122.0, 119.2, 116.1, 27.1, 26.5, 20.7, 19.3 ppm; IR (ATR): $\tilde{\nu}$ = 2932, 2858, 1584, 1563, 1547, 1477, 1333, 1307, 1265, 1107, 929, 701 cm^{-1}; HRMS (ESI+): m/z: [M+H]$^+$ calcd for C$_{45}$H$_{47}$BrNO$_2$Si$_2$ 770.2313; found: 770.2289.

(*E*)-2-[(3-bromo-4,5-dihydroxyphenyl)-1-ethenyl]pyridinium chloride (c2): Triethylamine trihydrofluoride (0.38 mL, 2.34 mmol) was added dropwise at 0°C to a solution of **7** (0.60 g, 0.78 mmol) in dry THF (10 mL). After the mixture had been stirred for 2 h at room temperature, 35% HCl was added (0.5 mL) and the resulting suspension was stirred for 10 min at room temperature and then filtered. The solid was washed with ethyl ether (2×5 mL) and dried under vacuum to afford (*E*)-2-[(3-bromo-4,5-dihydroxyphenyl)-1-ethenyl]pyridinium chloride (**c2**) as a yellow solid (0.166 g, 0.51 mmol; 65%). M.p. 210–212°C (acetone); ^{1}H NMR (360 MHz, [D$_6$]DMSO): δ = 10.44 (br s, 1H), 9.93 (br s, 1H), 8.70 (d, J = 5.0 Hz, 1H), 8.43 (t, J = 7.7 Hz, 1H), 8.26 (d, J = 8.3 Hz, 1H), 7.96 (d, J = 16.6 Hz, 1H), 7.75 (t, J = 6.8 Hz, 1H), 7.31 (d, J = 2.0 Hz, 1H),

7.19 ppm (d, $J = 2.0$ Hz, 1 H); ^{13}C NMR (90 MHz, [D$_6$]DMSO): $\delta = 150.5$, 146.6, 145.6, 144.8, 141.4, 139.2, 127.2, 124.0, 123.7, 123.5, 116.9, 113.2, 110.0 ppm; IR (ATR): $\tilde{v} = 3049$, 2811, 1637, 1614, 1593, 1429, 1296, 1163, 964, 830, 760 cm^{-1}; HRMS (ESI−): m/z: $[M - HCl - H^+]^-$ calcd for C$_{13}$H$_9$BrNO$_2$ 289.9822; found: 289.9817.

Crystal data: Owing to the low diffraction intensity of the crystals, the diffraction data were collected under synchrotron radiation ($\lambda = 0.977$ Å) at 150 K with a CCD detector in the BM16 Spanish beamline at the ESRF (Grenoble). The crystal was coated in paratone. The structure was solved by direct methods and refined by full-matrix least-squares techniques on $F2$ with SHELX-97.[30] Crystal adsorption was corrected by Scalepack.[31] Non-hydrogen atoms were refined anisotropically. Crystallographic details for **2**: $M_r = 441.84$, crystal size $0.3 \times 0.2 \times 0.03$, monoclinic phase, space group $P21/c$, $a = 9.975(2)$, $b = 20.793(3)$, $c = 16.760(2)$ Å, $V = 3578(5)$ Å^3, $Z = 8$, $\rho_{calcd} = 1.078$ g cm^{-3}, $F(000) = 23\,926$, $\mu(Mo_{K\alpha}) = 0.642$ mm^{-1}. A total of 17 129 reflections were measured in the range of $5.66 \leq 2\theta \leq 56.78°$, of which 13 560 were unique ($R_{int} = 0.0235$). Final R indices: $R1 = 0.0746$ $[I/2\sigma(I)]$, $wR2 = 0.1821$ (all data) for 682 parameters; max./min. residual electron density $0.733/-1.130$ e Å^{-3}.

Steady-state absorption and fluorescence spectroscopy: UV/Vis spectra were recorded at room temperature by using a Varian Cary05e spectrophotometer. Fluorescence spectra were recorded at room temperature in a Perkin Elemer LS 45 fluorescence spectrophotometer. The fluorescence quantum yields of all solutions investigated were determined relative to N,N'-bis(1-hexylheptyl)perylene-3,4,9,10 in acetonitrile ($\Phi_f = 1$).[28]

pH measurements: pH measurements upon acid–base addition to acetonitrile solutions of **1** and **2** were performed at room temperature with a Crison 52–01 pH electrode in a Crison BASIC 20 potentiometer. pH values are given relative to the acetonitrile solvent (^s_spH scale).[29] To calibrate the electrode system, we used reference buffer solutios in acetonitrile (pyridine–pyridinium bromide and phenol–sodium phenolate), whose ^s_spH can be derived from the Henderson–Hasselbach equation by using the pK_a values in acetonitrile reported for these systems.[29]

Quantum-chemical calculations: Quantum-chemical calculations were performed by employing the Gaussian 03 package of programs[30] on a 32-bit multiprocessor computer. DFT geometrical optimization of ground electronic states of all investigated molecules was carried out at the B3LYP hybrid functional level with the $6 – 311 + G(d,p)$ basis set. To account for solvent polarity effects, calculations were performed in acetonitrile solvent by means of the polarizable continuum model (PCM, $\varepsilon = 36.64$). The resulting geometries and molecular orbitals were plotted by using Molden. The excitation energies and oscillator strengths (f) of the UV/Vis absorption transition bands were then computed by means of time-dependent DFT at the B3LYP/6–311G + (d,p) level on the B3LYP/6–311 + G(d,p) ground-state geometries and accounting for acetonitrile solvent (PCM). For each protonation state of **1** and **2**, the spectroscopic properties of all possible rotamers were calculated and the final average values were obtained by using Boltzmann coefficients at room temperature ($\exp(-E_{rotamer}/k_BT)/\Sigma \exp(-E_{rotamer}/k_BT)$) as weighting factors.

Acknowledgements

[1] B. R. Eggins, *Chemical Senors and Biosensors (Analytical Techniques in the Sciences)*, Wiley-VCH, Weinheim, **2002**.

[2] a) *Fluorescent Chemosensors for Ion and Molecule Recognition* (Ed.: A. W. Czarnik), ACS Books, Washington, **1993**; b) A. P. de Silva, H. Q. N. Gunaratne, T. Gunnlaugsson, A. J. M. Huxley, C. P. McCoy, J. T. Rademacher, T. E. Rice, *Chem. Rev.* **1997**, *97*, 1515–1566; c) O. S. Wolfbeis, *J. Mater. Chem.* **2005**, *15*, 2657–2669; d) L. Basabe-Desmonts, D. N. Reinhoudt, M. Crego-Calama, *Chem. Soc. Rev.* **2007**, *36*, 993–1017.

[3] a) B. Valeur, I. Leray, *Coord. Chem. Rev.* **2000**, *205*, 3–40; b) P. D. Beer, P. A. Gale, *Angew. Chem. Int. Ed.* **2001**, *40*, 487–516; c) R. Martínez-Máñez, F. Sancenón, *Chem. Rev.* **2003**, *103*, 4419–4476; d) L. Fabbrizzi, M. Licehelli, A. Taglietti, *Dalton Trans.* **2003**, 3471–3479; e) G. W. Gokel, W. M. Leevy, M. E. Weber, *Chem. Rev.* **2004**, *104*, 2723–2750.

[4] a) J. W. Bell, N. M. Hext, *Chem. Soc. Rev.* **2004**, *33*, 589–598; b) R. Jelinek, S. Kolusheva, *Chem. Rev.* **2004**, *104*, 5987–6016.

[5] a) A. P. de Silva, R. A. D. D. Rupasinghe, *J. Chem. Soc. Chem. Commun.* **1985**, 1669–1670; b) S. G. Schulman, S. Chen, F. Bai, M. J. P. Leiner, L. Weis, O. S. Wolfbeis, *Anal. Chim. Acta* **1995**, *304*, 165–170; c) L. M. Daffy, A. P. de Silva, H. Q. N. Gunaratne, C. Huber, P. L. M. Lynch, T. Werner, O. S. Wolfbeis, *Chem. Eur. J.* **1998**, *4*, 1810–1815; d) S. Charier, O. Ruel, J.-B. Baudin, D. Alcor, J.-F. Allemand, A. Meglio, L. Jullien, *Angew. Chem.* **2004**, *116*, 4889–4892; *Angew. Chem. Int. Ed.* **2004**, *43*, 4785–4788; e) G. Nishimura, Y. Shiraishi, T. Hirai, *Chem. Commun.* **2005**, 5313–5315; f) A. S. Vasylevska, A. A. Karasyov, S. M. Borisov, C. Krause, *Anal. Bional. Chem.* **2007**, *387*, 2131–2141; g) A. P. de Silva, S. S. K. de Silva, N. C. W. Goonesekera, H. Q. N. Gunaratne, P. L. Lynch, R. K. Nesbitt, S. T. Patuwathavithana, N. L. D. Ramyalai, *J. Am. Chem. Soc.* **2007**, *129*, 3050–3051; h) B. Tang, X. Liu, K. Xu, H. Huang, G. Yang, L. An, *Chem. Commun.* **2007**, 3726–3728.

[6] a) D. Margulies, G. Melman, A. Shanzer, *Nat. Mater.* **2005**, *4*, 768–771; b) A. P. de Silva, S. Uchiyama, *Nat. Nanotechnol.* **2007**, *2*, 399–410.

[7] a) T. Gunnlaugsson, D. Parker, *Chem. Commun.* **1998**, 511–512; b) M. Su, H. Ma, Q. Ma, Z. Wang, J. Yang, M. Wang, *Chem. Commun.* **2001**, 960–961; c) F. Pina, J. C. Lima, C. Lodeiro, J. S. de Melo, P. Díaz, M. T. Albelda, E. García-España, *J. Phys. Chem. A* **2002**, *106*, 8207–8212; d) V. F. Valuk, G. Duportail, V. G. Pivovarenko, *J. Photochem. Photobiol. A* **2005**, *175*, 226–231; e) Y. Shiraishi, Y. Tokitoh, G. Nishimura, T. Hirai, *J. Phys. Chem. B* **2007**, *111*, 5090–5100.

[8] a) A. P. de Silva, H. Q. N. Gunaratne, C. P. McCoy, *Chem. Commun.* **1996**, 2399–2400; b) T. Gunnlaugsson, J. P. Leonard, K. Sénéchal, A. J. Harte, *J. Am. Chem. Soc.* **2003**, *125*, 12062–12063; c) S. A. de Silva, K. C. Loo, B. Amorelli, S. L. Pathirana, M. Nyakirangáni, M. Dharmasena, S. Demarais, B. Dorcley, P. Pullay, Y. A. Salih, *J. Mater. Chem.* **2005**, *15*, 2791–2795; d) Y. Diaz-Fernandez, F. Fori, C. Mangano, P. Pallavicini, S. Patroni, A. Perez-Gramatges, S. Rodriguez-Calvo, *Chem. Eur. J.* **2006**, *12*, 921–930.

[9] a) P. Pallavicini, V. Amendola, C. Massera, E. Mundum, A. Taglietti, *Chem. Commun.* **2002**, 2452–2453; b) V. Amendola, L. Fabbrizzi, C. Mangano, H. Miller, P. Pallavicini, A. Parotti, A. Taglietti, *Angew. Chem.* **2002**, *114*, 2665–2668; *Angew. Chem. Int. Ed.* **2002**, *41*, 2553–2556; c) Z. Wang, G. Zheng, P. Lu, *Org. Lett.* **2005**, *7*, 3669–3672; d) G. Zheng, Z. Wang, L. Tang, P. Lu, W. P. Weber, *Sens. Actuators B* **2007**, *122*, 389–394.

[10] R. Sjöback, J. Nygren, M. Kubista, *Spectrochim. Acta Part A* **1995**, *51*, L7 L21.

[11] R. J. Motekaitis, A. E. Martell, *Inorg. Chem.* **1984**, *23*, 18–23.

[12] E. Evangelio, D. Ruiz-Molina, *Eur. J. Inorg. Chem.* **2005**, *15*, 2957–2971.

[13] C. G. Pierpont, C. W. Lange, *Prog. Inorg. Chem.* **1994**, *41*, 331–443.

[14] S. Espinosa, E. Bosch, M. Rosés, *J. Chromatogr. A* **2002**, *964*, 55–66.

[15] As a proof-of-concept, the implementation of **2** in a nanostructured pH sensor and the performance of the resulting device has also already been reported in a previous communication: A. Martinez-Otero, E. Evangelio, R. Alibes, J. L. Bourdelande, D. Ruiz-Molina, F. Busque, J. Hernando, *Langmuir* **2008**, *24*, 2963–2966.

[16] R. G. Lange, *J. Org. Chem.* **1962**, *27*, 2037–2039.

[17] F. D. Lewis, E. M. Crompton, *J. Am. Chem. Soc.* **2003**, *125*, 4044–4045.

[18] E. M. Crompton, F. D. Lewis, *Photochem. Photobiol. Sci.* **2004**, *3*, 660–668.

[19] H. Ilhmels, A. Meiswinkel, C. J. Mohrschladt, D. Otto, M. Waidelich, M. Towler, R. White, M. Albrecht, A. Schnurpfeil. *J. Org. Chem.* **2005**, *70*, 3929–3938.

[20] I. M. Kolthoff, M. K. Chantoon, *J. Phys. Chem.* **1968**, *72*, 2270–2272.

[21] T. Murohoshi, K. Kaneda, M. Ikegami, T. Arai, *Photochem. Photobiol. Sci.* **2003**, *2*, 1247–1249.

[22] G. Favaro, U. Mazzucato, F. Masetti, *J. Phys. Chem.* **1973**, *77*, 601–604.

[23] G. Ginocchietti, U. Mazzucato, A. Spalletti, *Int. J. Photoenergy* **2004**, *6*, 241–250.

[24] U. Mazzucato, F. Momicchioli, *Chem. Rev.* **1991**, *91*, 1679–1719.

[25] a) B. Mennucci, *J. Am. Chem. Soc.* **2002**, *124*, 1506–1515; b) J. Tomasi, R. Cammi, B. Mennucci, C. Cappell, S. Corni, *Phys. Chem. Chem. Phys.* **2002**, *4*, 5697–5712.

[26] M. J. Kamlet, J. L. M. Abboud, M. H. Abraham and R. W. Taft, *J. Org. Chem.* **1983**, *48*, 2982–2996.

[27] G. Marconi, G. Bartocci, U. Mazzucato, A. Spalletti, F. Abbate, L. Angeloni, E. Castellucci, *Chem. Phys.* **1995**, *196*, 383–393.

[28] T. Kircher, H.-G. Löhmannsröben, *Phys. Chem. Chem. Phys.* **1999**, *1*, 3987–3992.

[29] S. Espinosa, E. Bosch, M. Rosés, *Anal. Chem.* **2000**, *72*, 5193–5200.

[30] Gaussian 03 (Revision B.04), M. J. Frisch, G. W. Trucks, H. B. Schlegel, G. E. Scuseria, M. A. Robb, J. R. Cheeseman, J. A. Montgomery, Jr., T. Vreven, K. N. Kudin, J. C. Burant, J. M. Millam, S. S. Iyengar, J. Tomasi, V. Barone, B. Mennucci, M. Cossi, G. Scalmani, N. Rega, G. A. Petersson, H. Nakatsuji, M. Hada, M. Ehara, K. Toyota, R. Fukuda, J. Hasegawa, M. Ishida, T. Nakajima, Y. Honda, O. Kitao, H. Nakai, M. Klene, X. Li, J. E. Knox, H. P. Hratchian, J. B. Cross, V. Bakken, C. Adamo, J. Jaramillo, R. Gomperts, R. E. Stratmann, O. Yazyev, A. J. Austin, R. Cammi, C. Pomelli, J. W. Ochterski, P. Y. Ayala, K. Morokuma, G. A. Voth, P. Salvador, J. J. Dannenberg, V. G. Zakrzewski, S. Dapprich, A. D. Daniels, M. C. Strain, O. Farkas, D. K. Malick, A. D. Rabuck, K. Raghavachari, J. B. Foresman, J. V. Ortiz, Q. Cui, A. G. Baboul, S. Clifford, J. Cioslowski, B. B. Stefanov, G. Liu, A. Liashenko, P. Piskorz, I. Komaromi, R. L. Martin, D. J. Fox, T. Keith, M. A. Al-Laham, C. Y. Peng, A. Nanayakkara, M. Challacombe, P. M. W. Gill, B. Johnson, W. Chen, M. W. Wong, C. Gonzalez, J. A. Pople, Gaussian, Inc., Wallingford CT, **2004**.

[31] G. M. Sheldrick, Program for the Refinement of Crystal Structures; University of Göttingen, Germany, **1997**.

[32] Z. Otwinowski, W. Minor, *Methods Enzymol.* **1997**, *276*, 307–326.